JOURNAL OF GEOPHYSICAL RESEARCH, VOL. ???, XXXX, DOI:10.1029/,

Generalized Analytical Model for Benthic Water Flux Forced by Surface-Gravity Waves

J. N. King

U. S. Geological Survey

Florida Integrated Science Center

Fort Lauderdale, Florida, USA

A. J. Mehta

R. G. Dean

Department of Civil and Coastal Engineering

University of Florida

Gainesville, Florida, USA

J. N. King, U. S. Geological Survey, Florida Integrated Science Center, 3110 S.W. 9^{th} Avenue, Fort Lauderdale, FL 33315, USA. (jking@usgs.gov)

A. J. Mehta and R. G. Dean, Department of Civil and Coastal Engineering, University of Florida, PO Box 116580, Gainesville, FL 32611, USA.

Abstract. A generalized analytical model for benthic water flux forced by linear surface-gravity waves over a series of layered, hydrogeologic units is developed by adapting a previous solution for a hydrogeologic unit with an infinite thickness (Case I) to a unit with a finite thickness (Case II), and to a dual-unit system (Case III). The model compares favorably with laboratory observations. The amplitude of wave-forced benthic water flux is shown to be directly proportional to the amplitude of the wave, permeability of the hydrogeologic unit, and the wave number; and inversely proportional to the kinematic viscosity of water. A dimensionless amplitude parameter is introduced and shown to reach a maximum where the product of water depth and the wave number is 1.2. Submarine groundwater discharge (SGD) is a benthic water discharge flux to a marine water body. The Case I model estimates an 11.5–cm/d SGD forced by a wave with a one second period and five centimeter amplitude, in water that is 0.5m deep. As this wave propagates into a region with a 0.3–m-thick hydrogeologic unit, with a no-flow bottom boundary, the Case II model estimates a 9.7–cm/d wave-forced SGD. As this wave propagates into a region with a 0.2–m-thick hydrogeologic unit over an infinitely thick, more permeable unit, the Case III quasi-confined model estimates a 15.7–cm/d wave-forced SGD. The quasi-confined model has benthic constituent flux implications in coral reef, karst, and clastic regions. Waves may undermine tracer and seepage meter estimates of SGD at some locations.

1. Introduction

Submarine groundwater discharge (SGD) has been the focus of numerous field, laboratory, and modeling investigations over the past decade. Field observations of SGD typically employ either seepage meters or naturally occurring tracers. *Taniguchi et al.* [2002] tabulated 45 SGD field studies on five continents; the tabulated studies used 20 different SGD characterization techniques. SGD estimates from these studies range from $8 \times 10^{-3}\, cm/d$ to $124\, cm/d$. Although most field studies are conducted at locations where surface-gravity waves are ubiquitous, waves are frequently ignored as a significant SGD forcing mechanism.

SGD is exclusively a marine process; in the current work, the more general term "benthic flux" is used in place of SGD to avoid this limitation. Benthic flux q_{bf} is the rate of flow of some property across the bed of a water body, per unit area of bed, with no limitation on the type of water body or direction of flow. Benthic flux is a vector quantity, where the vector is normal to the bed. Benthic discharge flux q_{bd} is oriented from the geologic domain to the surface-water domain, and benthic recharge flux q_{br} is oriented from the surface-water domain to the geologic domain (Figure 1), such that

$$q_{bf} = \begin{cases} q_{bd}, & q_{bf} > 0 \\ q_{br}, & q_{bf} < 0 \end{cases} \qquad (1)$$

The units of q_{bf} are a function of the property under consideration. For example, the units of a benthic volume flux are $[L^3T^{-1}L^{-2}] = [LT^{-1}]$, where $[L]$ is a length dimension and $[T]$ is a time dimension. SGD is then a benthic water discharge flux $q_{bd.w}$ to a marine water body.

The primary objective of the current work is to develop a generalized analytical solution for benthic water flux $q_{bf.w}$ forced by linear surface-gravity waves over layered strata, by employing *Reid and Kajiura*'s [1957] boundary value solution for linear-wave damping by a rigid, porous medium. Three specific cases of the generalized solution are developed (Figure 1): *Reid and Kajiura*'s [1957] hydrogeologic unit of infinite thickness (Case I), a unit of finite thickness (Case II), and a dual-unit system that consists of a unit of finite thickness over a unit of infinite thickness (Case III). A hydrogeologic unit is a zone of rock or soil that can be described with a single realization of representative parameters, which are typically used to quantify the flow of water in a porous medium, such as permeability k or porosity n. Although a single realization of a parameter, such as one k value, is used to describe a hydrogeologic unit, the unit is not necessarily homogeneous.

Reid and Kajiura [1957] showed that a wave loses energy to "percolation" as the wave propagates across a porous medium. *Reid and Kajiura*'s [1957] percolation is a benthic water flux, forced by the pressure gradient at the bed. *Reid and Kajiura* [1957] used a complex wave number

$$\lambda = \lambda_r + \imath\lambda_\imath \tag{2}$$

where $\lambda_r = 2\pi/L$ and $\lambda_\imath$ are real and imaginary components, and L is wave length, to show that wave amplitude a is damped by $e^{-\lambda_\imath x}$ over some distance x, such that $a(x > 0) = a(x = 0)e^{-\lambda_\imath x}$.

Riedl et al. [1972] showed that the observed amplitude of $q_{bf.w}$ ($2.5 \times 10^{-5}\ m/s$ to $6.0 \times 10^{-5}\ m/s$ off Bogue Bank, North Carolina, USA) compared favorably with an amplitude predicted with *Reid and Kajiura* [1957] ($3.0 \times 10^{-5}\ m/s$); and identified the phenomenon as subtidal pumping. *Riedl et al.* [1972] did not parse observed $q_{bf.w}$ off Bogue Bank into components forced by waves and components forced by other processes.

The current work generalizes the existing solution for one hydrogeologic unit of infinite thickness, to address a series of layered units. *Reid and Kajiura*'s [1957] use of the term "infinite" may be misleading to some readers. It will be shown in Section 6.1, after the development of necessary mathematics, that $q_{bf.w}$ on a hydrogeologic unit of finite thickness $\hat{h}$ approaches $q_{bf.w}$ on a hydrogeologic unit of infinite thickness, where $\lambda_r \hat{h} > \pi$. Note that the product $\lambda_r \hat{h}$—dimensionless hydrogeologic unit thickness—includes both wave (λ_r) and hydrogeologic unit ($\hat{h}$) characteristics.

Secondary objectives of the current work are to (1) validate the solution using laboratory data from *Yamamoto et al.* [1978], and (2) examine the role that wave length, wave period, hydrogeologic unit thickness, water depth, and permeability play in damping or amplifying wave-forced $q_{bf.w}$. A practical example is presented to show that small-amplitude waves force $O(10cm/d)$ SGD. Finally, the possibility that waves may confound tracer and seepage meter estimates of SGD is discussed.

2. Benthic Flux Boundary Value Problem

Reid and Kajiura [1957] solved a two-dimensional boundary value problem in horizontal x and vertical z dimensions (Figure 1A). The bed is horizontal and planar, with a normal oriented parallel to the gravity vector. The porous medium is homogeneous and isotropic. Flow in the surface-water domain is irrotational and inviscid. Flow in the porous domain is laminar and viscous. A low-amplitude, linear wave forces a water-surface displacement $\eta = ae^{\imath(\lambda x - \sigma t)}$ about the still-water surface at $z = 0$, where $\sigma = 2\pi/T$ is wave radial frequency, T wave period, and t is time. Total pressure p_{total} is parsed into static p_{static}

and dynamic p components, such that

$$\begin{aligned} p_{total} &= p + p_{static} \\ &= p - \rho g z \end{aligned} \quad (3)$$

where ρ is the density of water and g is gravitational acceleration. Governing equations are the Laplacian ∇^2 of the velocity potential $\phi(x, z, t)$ in the surface-water domain and dynamic pressure $p_{pm}(x, z, t)$ in the porous medium

$$\nabla^2 \phi = 0 \quad (4)$$

$$\nabla^2 p_{pm.j} = 0 \quad (5)$$

where the subscript $_{pm}$ identifies a porous-medium variable and the subscript $_j$ is a hydrogeologic unit counter ($j = 1$ for the unit bounded by $z = -h$). Dynamic and kinematic boundary conditions constrain the solution at (1) the free surface ($z = \eta$):

$$\eta = \frac{1}{g}\frac{\partial \phi}{\partial t} \quad (6)$$

$$w = \frac{\partial \eta}{\partial t} \quad (7)$$

where w is vertical, z-oriented velocity; (2) the bed ($z = -h$):

$$p = p_{pm.(j=1)} \quad (8)$$

$$w = w_{pm.(j=1)} \quad (9)$$

where the absence of a subscript on the left-hand-side of the equation denotes a variable in the surface-water domain; and (3) the interface of two hydrogeologic units (for example: $z = -h - \hat{h}$ in Figure 1C):

$$p_{pm.j} = p_{pm.(j+1)} \quad (10)$$

$$w_{pm.j} = w_{pm.(j+1)} \quad (11)$$

A no-flow boundary condition $w_{pm} = 0$ exists at the base of the deepest unit. If the deepest unit is infinitely thick, then $w_{pm}(z \to -\infty) = 0$.

3. Generalized Solution

It can be shown that

$$\begin{aligned} p_{pm} &= f\left(\lambda h, \lambda \hat{h}_j, k_j, \frac{\sigma}{\nu}\right) \frac{\rho g a}{\cosh \lambda h} e^{\imath(\lambda x - \sigma t)} \\ &\quad \times \left[\delta_c \cosh(\lambda h + \lambda z + \sum \lambda \hat{h}_j) + \delta_s \sinh(\lambda h + \lambda z + \sum \lambda \hat{h}_j)\right] \end{aligned} \tag{12}$$

satisfies Equation 5, where f is a dimensionless function of hydrogeologic-unit characteristics, h depth from the still-water surface to the bed, $\hat{h}_j$ finite thickness of hydrogeologic unit j, k_j permeability of hydrogeologic unit j, ν kinematic viscosity of water, and δ_c and δ_s are binary functions of hydrogeologic unit geometry, which take the value 0 or 1. It can be shown with Equation 12 that

$$q_{bf.w.nd} = \frac{q_{bf.w}}{\alpha} = -\cos(\lambda_r x - \sigma t) + \beta \sin(\lambda_r x - \sigma t) \tag{13}$$

where $q_{bf.w.nd}$ is dimensionless $q_{bf.w}$ forced by waves,

$$\alpha = \frac{\hat{P} a g k \lambda_r e^{-\lambda_\imath x}}{\nu \cosh(\lambda_r h)} \tag{14}$$

is $q_{bf.w}$ amplitude,

$$\beta = \tanh(\lambda_r h)(\hat{P} R - \lambda_\imath h) + \frac{\lambda_\imath}{\lambda_r} + \hat{Q} \tag{15}$$

is $q_{bf.w}$ amplification parameter, $\hat{P}$ and $\hat{Q}$ are dimensionless model parameters that change with model geometry, and

$$R = \frac{\sigma k}{\nu} \tag{16}$$

is *Reid and Kajiura*'s [1957] fundamental dimensionless permeability modulus. Increases in permeability cause R to increase; increases in wave period and viscosity cause R to decrease. Equation 13 is plotted in Figure 2: where $\beta = 0$, the extrema in the wave surface correspond with the mirrored extrema in q_{bf}, such that maximum q_{br} occurs at the wave crest and maximum q_{bd} occurs at the trough. The role that β plays in amplifying $q_{bf.w.nd}$ is discussed in Section 6.3. The generalized dispersion equation

$$\sigma^2 - g\lambda \tanh(\lambda h) = -\imath \hat{P} R \left[g\lambda - \sigma^2 \tanh(\lambda h) \right] \tag{17}$$

relates σ and λ. Substitution of Equation 2 into Equation 17 yields

$$\sigma^2 \approx g\lambda_r \tanh(\lambda_r h) \tag{18}$$

$$\lambda_\imath \approx \frac{2\hat{P}R\lambda_r}{2\lambda_r h + \sinh(2\lambda_r h)} \tag{19}$$

Equation 18 is the well-known dispersion equation, which relates T to L, such that changes in σ are implicitly tied to conclusions based on dimensionless parameters in λ_r. Equation 18 is not a function of porous domain geometry, and is therefore valid for all cases. Equation 19 is a function of porous domain geometry because it includes the dimensionless model parameter $\hat{P}$.

4. Specific Solutions

4.1. Case I: Hydrogeologic Unit with Infinite Thickness

Reid and Kajiura [1957] assumed the following forms of the solution

$$\phi(x,z,t) = \left[A \cosh(\lambda h + \lambda z) + B \sinh(\lambda h + \lambda z)\right] e^{\imath(\lambda x - \sigma t)} \tag{20}$$

$$p_{pm}(x,z,t) = C e^{\lambda h + \lambda z} e^{\imath(\lambda x - \sigma t)} \tag{21}$$

which satisfy Equations 4, 5, and $w_{pm}(z \to -\infty) = 0$ (Figure 1A). Their solution employs Bernoulli's equation

$$p = \rho \frac{\partial \phi}{\partial t} \tag{22}$$

the definition of the velocity potential

$$w = -\frac{\partial \phi}{\partial z} \tag{23}$$

and Darcy's Law

$$w_{pm} = \frac{-k}{\mu} \frac{\partial p_{pm}}{\partial z} \tag{24}$$

where μ is the dynamic viscosity of water, to yield four equations (Equations 6, 7, 8, and 9) and four unknowns (A, B, C, and λ), such that

$$\sigma^2 - g\lambda \tanh(\lambda h) = -\imath R \left[g\lambda - \sigma^2 \tanh(\lambda h) \right] \tag{25}$$

Latin-lettered unknowns are presented in the Appendix, for all cases.

Substitution of Equation 2 into Equation 25 yields Equation 18 and

$$\lambda_\imath \approx \frac{2R\lambda_r}{2\lambda_r h + \sinh(2\lambda_r h)} \tag{26}$$

This development exploits the fact that the product of small terms ($\lambda_\imath \ll 1$ and $R \ll 1$) is negligible, such that $\lambda_\imath R \approx 0$, $R^2 \approx 0$, $\lambda_\imath^2 \approx 0$; and that asymptotic approximations exist for hyperbolic trigonometric operations on small terms, such that $\sinh(\imath\lambda_\imath h) \approx \imath\lambda_\imath h$, and $\cosh(\imath\lambda_\imath h) \approx 1$. Equations 21, 24, and A3 yield

$$q_{bf.w.I} = \Re[w_{pm}] = -\alpha_I \left[\cos(\lambda_r x - \sigma t) - \beta_I \sin(\lambda_r x - \sigma t)\right] \tag{27}$$

where $\hat{P} = 1$, $\hat{Q} = 0$,

$$\alpha_I = \frac{agk\lambda_r e^{-\lambda_\imath x}}{\nu \cosh(\lambda_r h)} \tag{28}$$

$$\beta_I = \tanh(\lambda_r h)(R - \lambda_\imath h) + \frac{\lambda_\imath}{\lambda_r} \tag{29}$$

Case-specific solution components are referenced in the current work with subscript $_I$ for Case I, $_{II}$ for Case II, and $_{III}$ for Case III. Dimensionless model parameters $\hat{P}$ and $\hat{Q}$

are detailed for each case in Table 1. Example applications are detailed for each case in Section 7.

4.2. Case II: Hydrogeologic Unit with Finite Thickness

To adapt *Reid and Kajiura*'s [1957] solution (Case I) to a hydrogeologic unit with a finite thickness (Case II; Figure 1B), assume solutions of the form

$$\phi(x,z,t) = [A\cosh(\lambda h+\lambda z)+B\sinh(\lambda h+\lambda z)]\, e^{\imath(\lambda x-\sigma t)} \tag{30}$$

$$p_{pm}(x,z,t) = \left[C\cosh(\lambda h+\lambda\hat{h}+\lambda z)+D\sinh(\lambda h+\lambda\hat{h}+\lambda z)\right] e^{\imath(\lambda x-\sigma t)} \tag{31}$$

which satisfy Equations 4 and 5. Use the no-flow boundary $w_{pm}(z=-h-\hat{h})=0$. Solve the system of five equations (Equations 6, 7, 8, 9, and the no-flow boundary condition) and five unknowns (A, B, C, D, λ) to yield

$$\sigma^2 - g\lambda\tanh(\lambda h) = -\imath\hat{P}_{II}R\left[g\lambda-\sigma^2\tanh(\lambda h)\right] \tag{32}$$

$$\hat{P}_{II} = \tanh(\lambda_r\hat{h}) \tag{33}$$

$$\lambda_\imath \approx \frac{2\hat{P}_{II}R\lambda_r}{2\lambda_r h+\sinh(2\lambda_r h)} \tag{34}$$

$$q_{bf.w.II} = \Re[w_{pm}] = -\alpha_{II}\left[\cos(\lambda_r x-\sigma t)-\beta_{II}\sin(\lambda_r x-\sigma t)\right] \tag{35}$$

$$\alpha_{II} = \frac{\hat{P}_{II}agk\lambda_r e^{-\lambda_\imath x}}{\nu\cosh(\lambda_r h)} \tag{36}$$

$$\beta_{II} = \tanh(\lambda_r h)(\hat{P}_{II}R-\lambda_\imath h)+\frac{\lambda_\imath}{\lambda_r}+\hat{Q}_{II} \tag{37}$$

$$\hat{Q}_{II} = \frac{2\lambda_\imath\hat{h}}{\sinh(2\lambda_r\hat{h})} \tag{38}$$

The Case II solution must become approximately equal to the Case I solution where the hydrogeologic unit of finite thickness becomes very thick. Restated, the generalized model exhibits case congruence with convergent hydrogeologic-unit properties. Specifically, Case II to Case I congruence occurs as $\hat{h} \to \infty$ (the unit becomes thick), such that $\hat{P}_{II} \to 1$, $\hat{Q}_{II} \to 0$, and Case II model elements (Equations 32 and 35) reduce to Case I model elements (Equations 25 and 27)—or the Case II solution becomes approximately equal to the Case I solution.

4.3. Case III: Two-Layer System

To adapt *Reid and Kajiura*'s [1957] solution (Case I) to a two-layer system (Case III; Figure 1C), which consists of a hydrogeologic unit (identified with subscript $_1$) with a finite thickness over a hydrogeologic unit (identified with subscript $_2$) with an infinite thickness, specify governing equations for p_{pm} in both hydrogeologic units

$$\nabla^2 p_{pm1} = 0 \tag{39}$$

$$\nabla^2 p_{pm2} = 0 \tag{40}$$

and assume the solution presented in Equation 30, with additional solutions of the form

$$p_{pm1}(x,z,t) = \left[C\cosh(\lambda h + \lambda\hat{h} + \lambda z) + D\sinh(\lambda h + \lambda\hat{h} + \lambda z)\right] e^{\imath(\lambda x - \sigma t)} \tag{41}$$

$$p_{pm2}(x,z,t) = Ee^{\lambda h + \lambda\hat{h} + \lambda z} e^{\imath(\lambda x - \sigma t)} \tag{42}$$

such that p_{pm2} satisfies $w_{pm}(z \to -\infty) = 0$. Solve the system of six equations (Equations 6, 7, 8, 9, 10, and 11) and six unknowns (A, B, C, D, E, λ) such that

$$\sigma^2 - g\lambda\tanh(\lambda h) = -\imath\hat{P}_{III}R_1\left[g\lambda - \sigma^2\tanh(\lambda h)\right] \tag{43}$$

$$\hat{P}_{III} = \frac{\tanh(\lambda_r\hat{h}) + \frac{k_2}{k_1}}{\frac{k_2}{k_1}\tanh(\lambda_r\hat{h}) + 1} \tag{44}$$

$$\lambda_\imath \approx \frac{2\hat{P}_{III}R_1\lambda_r}{2\lambda_r h + \sinh(2\lambda_r h)} \tag{45}$$

$$R_1 = \frac{\sigma k_1}{\nu} \tag{46}$$

$$q_{bf.w.III} = \Re[w_{pm}] = -\alpha_{III}\left[\cos(\lambda_r x - \sigma t) - \beta_{III}\sin(\lambda_r x - \sigma t)\right] \tag{47}$$

$$\alpha_{III} = \frac{\hat{P}_{III} k_1 a g \lambda_r e^{-\lambda_\imath x}}{\nu \cosh(\lambda_r h)} \tag{48}$$

$$\beta_{III} = \tanh(\lambda_r h)(\hat{P}_{III} R_1 - \lambda_\imath h) + \frac{\lambda_\imath}{\lambda_r} + \hat{Q}_{III} \tag{49}$$

$$\hat{Q}_{III} = \frac{\lambda_\imath \hat{h}(1 - \frac{k_2}{k_1})\left[1 - \tanh^2(\lambda_r \hat{h})\right]}{\left[\frac{k_2}{k_1}\tanh(\lambda_r \hat{h}) + 1\right]\left[\tanh(\lambda_r \hat{h}) + \frac{k_2}{k_1}\right]} \tag{50}$$

where k_2/k_1 is the dimensionless permeability ratio (Figure 3).

The Case III solution must become approximately equal to the Case I solution where the hydrogeologic unit of finite thickness becomes very thin. Restated, Case III to Case I congruence occurs as $\hat{h} \to 0$ (the unit becomes thin), such that $(k_2/k_1) \to 1$, $\hat{P}_{III} \to 1$, $\hat{Q}_{III} \to 0$ and Case III model elements (Equations 43 and 47) reduce to Case I model elements (Equations 25 and 27)—or the Case III solution becomes approximately equal to the Case I solution.

The Case III solution must become approximately equal to the Case II solution where the permeability of the hydrogeologic unit of finite thickness becomes much larger than the permeability of the underlying unit. Restated, Case III to Case II congruence occurs where $(k_2/k_1) \ll 1$ (permeability of unit of finite thickness much larger than permeability of underlying unit), such that $\hat{P}_{III} \to \hat{P}_{II}$, $\hat{Q}_{III} \to \hat{Q}_{II}$ and Case III model elements (Equations 43 and 47) reduce to Case II model elements (Equations 32 and 35)—or the Case III solution becomes approximately equal to the Case II solution.

5. Comparison with Laboratory Observations

Yamamoto et al. [1978] used a flume with a 0.50 m-deep sediment trench centered on the bottom to measure wave-forced pore pressure response on $z < -h$. *Sleath* [1970] conducted similar work. *Yamamoto et al.*'s (1978) bed was saturated with water, with no entrained gas within the porous matrix, such that the pore fluid was incompressible.

Yamamoto et al. [1978] reported $|p(z < -h)|/p(z = -h)$, which can also be determined analytically for a flume

$$\frac{|p(z < -h)|}{p(z = -h)} = \frac{\cosh\left[\lambda_r(h + \hat{h} + z)\right]}{\cosh(\lambda_r \hat{h})} \tag{51}$$

by employing Case II (Equations 2, 31, A6, and A7) at $x = 0$.

Equation 51 compares favorably with *Yamamoto et al.*'s [1978] observations in a 1.2–mm-diameter, sand medium (Figure 4). Observational inputs are detailed in Table 2, outputs in Table 3. Coefficients of determination are 0.998, 0.996, 0.991, and 0.970 for the 1.0, 1.5, 2.0, and 2.6 s waves, respectively. The 1 s wave is a deep-water wave ($\pi < \lambda_r h$); the 1.5, 2.0, and 2.6 s waves are intermediate depth waves ($\pi/10 < \lambda_r h < \pi$). No definitive conclusion can be offered with respect to the weak decreasing trend in the coefficient of determination, as a function of T. This trend may correlate with a higher level of noise in the observational system, as a function of T. Unfortunately, it is not possible to calculate α or plot $q_{bf.w}$ because *Yamamoto et al.* [1978] did not report a.

6. Discussion

6.1. Infinite Thickness and a Cutoff between Cases I and II

Reid and Kajiura's [1957] assumption of a hydrogeologic unit of "infinite" thickness may be misleading to some readers. the current work shows that Case I is relevant where a finite hydrogeologic unit is sufficiently thick, such that $\tanh(\lambda_r \hat{h}) \approx 1$. Case II is necessary where $\tanh(\lambda_r \hat{h}) < 1$. It is possible for the relevant solution to transition from Case II to Case I in time at a particular location as λ_r increases, or in space along a particular wave ray as $\hat{h}$ and/or λ_r increase. For example, $\hat{P}_{II} = \tanh(\lambda_r \hat{h}) > 0.996$ and $\alpha_{II} \to \alpha_I$, where $\lambda_r \hat{h} > \pi$. However, as $\lambda_r \hat{h}$ continues to increase, $\tanh(\lambda_r \hat{h})$ never exceeds unity.

The hydrogeologic unit of finite thickness, with $\lambda_r \hat{h} > \pi$, behaves like a unit of infinite thickness, with $\lambda_r \hat{h} \to \infty$.

6.2. Dimensionless Amplitude Parameter for Benthic Water Flux

The dimensionless amplitude parameter for $q_{bf.w}$

$$\hat{A} = \frac{\alpha \nu h}{agk} = \frac{\lambda_r h \hat{P}}{\cosh(\lambda_r h)} \tag{52}$$

is developed using Equation 14 at $x = 0$. The right-hand side of Equation 52 is a function of dimensionless depth $\lambda_r h$, $\lambda_r \hat{h}$, and k_2/k_1. A maximum $\hat{A}$ exists at the intermediate depth $\lambda_r h = 1.2$, as shown in Figure 5 for Cases I and II, and in Figure 6 for Cases I and III. Case I is represented in both figures with $\lambda_r \hat{h} \to \infty$.

For $\lambda_r \hat{h} \to$ finite, $\hat{A}$ decreases under Case II, from a Case I maximum of 0.663 (Figure 5). For Case III, $\hat{A}$ increases or decreases, as a function of k_2/k_1, from the Case I maximum: $\hat{A}$ increases (Figures 6C and 6D) where $(k_2/k_1) > 1$ (quasi-confined system, Figure 3A); $\hat{A}$ decreases (Figures 6A and 6B) where $(k_2/k_1) < 1$ (quasi-finite system, Figure 3B). The dimensionless model parameter $\hat{P}$ modifies $\hat{A}_I$ to generate $\hat{A}_{II}$ and account for the finite hydrogeologic unit thickness of Case II. Because $\hat{P}_{II} < \hat{P}_I = 1$, $\alpha_{II} < \alpha_I$ for equivalent $\lambda_r h$ (Figure 5).

Where $(k_2/k_1) < 1$, such as a location where a clay unit of low k is overlain by a sand unit of high k (quasi-finite system, Figure 3B), the underlying unit of lower permeability (k_2) acts as a semi-impermeable bed, such that Case III becomes a quasi-finite-thickness version of Case II, $\hat{P}_{III} < \hat{P}_I = 1$, and $\alpha_{III} < \alpha_I$ for equivalent $\lambda_r h$ (Figure 6A and B). For Case III, where $(k_2/k_1) > 1$, such as a location where a karst unit of high k is overlain by a consolidated sediment unit of low k (quasi-confined system, Figure 3A), the semi-impermeable confining unit of lower permeability (k_1) amplifies α, such that $\hat{P}_{III} > \hat{P}_I = 1$ and $\alpha_{III} > \alpha_I$ (Figure 6C and D).

Cases I and III are congruent at $(k_2/k_1) = 1$. As k_2/k_1 deviates from unity, $\left|\partial\hat{A}/[\partial(\lambda_r\hat{h})]\right|$ increases, such that $\left|\partial\hat{A}/[\partial(\lambda_r\hat{h})]\right|_{(k_2/k_1)=0.1} < \left|\partial\hat{A}/[\partial(\lambda_r\hat{h})]\right|_{(k_2/k_1)=0.01}$ in Figures 6A and 6B, and $\left|\partial\hat{A}/[\partial(\lambda_r\hat{h})]\right|_{(k_2/k_1)=10} < \left|\partial\hat{A}/[\partial(\lambda_r\hat{h})]\right|_{(k_2/k_1)=100}$ in Figures 6C and 6D. Physically, $\lambda_r\hat{h}$ plays a more significant role in governing $\hat{A}$, as k diverges in each unit of the dual-unit system.

It is clear from Darcy's Law that p_{static} does not force $q_{bf.w}$. For shallow-water waves ($\lambda_r h < \pi/10$), $\hat{A}$ decreases from the intermediate-depth maximum (Figures 5 and 6) because the pressure distribution is dominated by the static component. For deep-water waves ($\lambda_r h > \pi$), $\hat{A}$ decreases from the intermediate-depth maximum because wave orbitals lose contact with the bed.

6.3. Benthic Water Flux Amplification Parameter

Examination of Figure 2 and Equation 13 show that $\beta > 0$ amplifies $q_{bf.w}$ and causes the time to maximum $q_{bf.w}$ to lag $q_{bf.w}$ at $\beta = 0$. However, under typical conditions (such as the conditions detailed in Table 4) $\beta < 0.1$, and Equation 13 reduces to

$$q_{bf.w.nd} \approx -\cos(\lambda_r x - \sigma t) \tag{53}$$

The reduced approximation is not valid where $\beta > 0.1$ [*King*, 2007, Figure 4-6], which occurs on $R > O(10^{-1})$, $R = O(10^{-2})$ and $\lambda_r h < O(0.1)$, or $R = O(10^{-3})$ and $\lambda_r h < O(0.01)$. For example, consider hydrogeologic units of 1–cm-diameter gravel ($k = 10^{-7} m^2$) and 1–mm-diameter sand ($k = 10^{-9}\, m^2$). With $\nu = 10^{-6}\, m^2/s$, $h = 0.5\, m$, and $T = 1\, s$: then (1) $\beta = 0.57$ (Equation 15), $R = 0.63$ (Equation 16), and the amplitude of $q_{bf.w.nd}$

is 1.15 for the 1–cm gravel (Equation 13, Figure 2); (2) $\beta = 0.0057$, $R = 0.0063$, and the amplitude of $q_{bf.w.nd}$ is 1.00 for the 1–mm sand. The gravel yields $\beta > 0.1$ and amplifies $q_{bf.w.nd}$ by 15%, in the same wave climate. A similar conclusion can be drawn for a longer period wave and a different set of additional parameters: $T = 4\,s$, $\nu = 10^{-6}m^2/s$, $h = 4m$, $k = 5 \times 10^{-7}m^2$ for gravel and $k = 5 \times 10^{-7}m^2$ for sand: then (1) $R = 0.79$, $\beta = 0.65$, and the amplitude of $q_{bf.w.nd} = 1.19$ for the gravel; (2) $R = 0.0079$, $\beta = 0.0065$, and the amplitude of $q_{bf.w.nd} = 1.00$ for the sand. The gravel in the second example also yields $\beta > 0.1$ and amplifies $q_{bf.w.nd}$ by 19%. Different sediment properties and wave climates may yield different conclusions.

6.4. Simple Model for Wave-Forced Benthic Constituent Flux

Wave-forced $q_{bf.w}$ integrates to zero over one wave period at a point on the bed,

$$\bar{q}_{bf.w} = \frac{1}{T}\int_0^T q_{bf.w}dt = 0 \tag{54}$$

However, for some constituents, the benthic constituent flux driven by $q_{bf.w}$ may not integrate to zero over one wave period at a point on the bed because constituent concentrations in surface waters may not be equivalent to concentrations in the hydrogeologic unit, near the bed.

The average $q_{bd.w}$ generated by the $q_{bf.w}$ signal over one wave period is

$$\bar{q}_{bd.w} = \frac{1}{T}\int_{\frac{T}{4}}^{\frac{3T}{4}} q_{bf.w}dt = \frac{\alpha}{\pi} \tag{55}$$

where $\beta = 0$. Integration is limited to the discharge portion ($[\sigma T/4] \rightarrow [3\sigma T/4]$) of $q_{bf.w}$, such that $\bar{q}_{bd.w} = -\bar{q}_{br.w}$. Average $q_{bd.w}$ over one wave period is equivalent to average, wave-forced SGD over the period.

Wave-forced w_{pm} within the hydrogeologic unit diminishes with depth into the bed, as $z \to -\infty$. It can be shown with Equations 2, 21, 24, and A3 that the ratio of vertical velocity at $z = (-h - \zeta)$ to vertical velocity at the bed is

$$\frac{w_{pm}(z = -h - \zeta)}{q_{bf.w}} \approx e^{-\lambda_r \zeta} \tag{56}$$

for Case I, where ζ is the thickness of the region of porous medium over which the wave-forced velocity field transports constituents (Figure 1A). If $[w_{pm}(z = -h - \zeta) / q_{bf.w}] = e^{-2\pi}$ then $\zeta \approx L$, where $e^{-2\pi}$ is both small and mathematically convenient.

Consider a rectangular, differential control volume of unit (horizontal) cross-sectional area, in which the bottom face of the control volume is aligned with the bed, and the top face of the control volume is in the surface-water domain, at a vertical height Δz above the bed,

$$\begin{aligned} Q_\chi &= \bar{q}_{bd.w} C_{bd.\chi} + \bar{q}_{br.w} C_{br.\chi} = \frac{\Delta C_\chi \Delta z}{\Delta t} \\ &= \bar{q}_{bd.w} (C_{bd.\chi} - C_{br.\chi}) \end{aligned} \tag{57}$$

is a mass conservation statement about the control volume for a non-reactive constituent χ of $q_{bf.w}$, where Q_χ is the rate of wave-forced mass-transport of χ, per unit area of bed; and $C_{bd.\chi}$ and $C_{br.\chi}$ are representative concentrations of χ in $q_{bd.w}$ and $q_{br.w}$, respectively. The surface-water domain is loaded with χ where $Q_\chi > 0$. Equation 57 is not appropriate where χ undergoes chemical or geochemical reactions during transport.

6.5. Model Limitations

A model of a natural system is usually an abstraction of a more complex prototype, with a soluble system of less complexity. The abstraction process requires assumptions, which can lead to limitations. The current model for $q_{bf.w}$ assumes a two-dimensional

x-z oriented system; linear wave; incompressible pore fluid; irrotational, inviscid flow in the surface-water domain; horizontal, plane bed; rigid, homogeneous, isotropic, porous medium; laminar and viscous flow in the porous medium; case-specific, no-flow boundary conditions; Darcy's Law; Equations 4 to 11; $\lambda_\imath \ll 1$; $R \ll 1$; and the hydrogeologic-unit concept. In a strict sense, some of these assumptions, such as a two-dimensional system, are never valid for practical applications. The abstraction process permits conclusions about the prototype to be drawn from the behavior of the model. Clearly, because *Riedl et al.* [1972] showed agreement between model a and observed a off Bogue Bank; and Equation 51 compares favorably with *Yamamoto et al.* [1978], it is possible to draw some meaningful conclusions about these natural or laboratory systems from the abstracted model.

For every application, users of these models must determine the degree to which abstraction influences conclusions. For example, non-linear wave crests are steeper and more narrow than linear wave crests. Non-linear wave troughs are more shallow and more elongated than linear wave troughs. A wave-pumping effect clearly exists for the linear wave (Figure 2). This effect will also exist for the non-linear wave, where, intuitively, the steeper non-linear wave crest will translate into a more negative, steeper $q_{bf.w.nd}$ trough; and the more shallow non-linear wave trough will translate into a less positive, elongated $q_{bf.w.nd}$ peak. The abstraction associated with representing a non-linear wave with a linear wave model may then introduce some error in extrema estimation. Equation 54, however, is valid for both linear and non-linear waves.

Benthic water flux is forced by multiple gradients in a natural system. For example, numerous investigators have considered the component of q_{bf} forced by wave-generated flows on rippled beds [*Shum*, 1992; *Precht and Huettel*, 2003; *Precht et al.*, 2004; *Precht and Huettel*, 2004; *Pilditch and Miller*, 2006]. Wave-forced $q_{bf.w}$ in a natural system might then be a combination of both the flow—rippled bed interaction and the percolation mechanism of *Reid and Kajiura* [1957]. Except where noted, $q_{bf.w}$ is exclusively forced throughout the current work by waves on a horizontal, plane bed, using the models detailed herein. Users of these models in natural systems are cautioned that $q_{bf.w}$ described by these models is only one component of an array of potential forcing mechanisms that may exist in a natural system.

7. Example Application

The following hypothetical example demonstrates the utility of the generalized model by showing that a typical, ubiquitous, small-amplitude wave ($T = 1\,s$, $a = 0.05\,m$) generates an $O(10\,cm/d)$ SGD in knee-deep water ($h = 0.5\,m$). This wave might be common during an SGD field study.

Consider the near-shore location described in Table 4 (Case I, $\lambda_r \hat{h} > \pi$). The 1 s wave is an intermediate-depth wave in 0.5 m of water ($[\pi/10] < \lambda_r h = 2.1 < \pi$). The dimensionless amplitude parameter $\hat{A}_I = 0.51$ at $\lambda_r h = 2.1$ (Equation 52 and Figure 5) is less than the maximum dimensionless amplitude parameter, $\hat{A}_{I.max} = 0.66$ at $\lambda_r h = 1.2$, because the benthic pressure gradient diminishes at this location, as wave orbitals lose contact with the bed. The parameter will maximize for this wave if h decreases to $0.25\,m$ with $T = 1\,s$, or if T increases to $1.4\,s$ with $h = 0.5\,m$. Small terms necessary to simplify the dispersion equation for this wave are of the appropriate magnitude ($R = O[10^{-5}] \ll 1, \lambda_{\imath.I} = O[10^{-5}]m^{-1} \ll 1\,m^{-1}$). Equation 53 is valid, with $\beta_I < 0.1$. Equations 14 or 52 yield $\alpha_I = 36.1\ cm/d$. (It is shown in Table 4 that an identical $\alpha_I = 36.1\ cm/d$ is generated where $T = 5\ s$, $a = 0.233\ m$, $h = 2.5\ m$; and where $T = 10\ s$, $a = 0.611\ m$, $h = 5.0\ m$.) For the 1 s wave, an increase in a, decrease in h, or increase in T to a maximum of 1.4 s will cause α_I to increase. Decreases in h can be forced by tide, or by episodic events. If $q_{bf.w}$ constituent concentrations are not equivalent in $q_{bd.w}$ and $q_{br.w}$, then $\bar{q}_{bd.w} = -\bar{q}_{br.w} = 11.5\ cm/d$ will cause a net advective constituent flux.

Assume that a hypothetical ^{222}Rn activity of 2 dpm/l (analogous to concentration) is representative of the activity in $q_{bd.w}$ at this location. (For comparison, over a one year period, *Martin et al.* [2006] observed ^{222}Rn activities up to 40 dpm/l at a depth of 10 cm below the bed, in the Indian River Lagoon, Florida.) Radon 222—a noble gas—is inert and non-reactive; atmospheric evasion and rapid radioactive decay result in a negligible ^{222}Rn activity in surface water. Equation 57 yields wave-forced $Q_{bd.I} = 230\ dpm/m^2d$ for ^{222}Rn, at this hypothetical location. At locations where ^{222}Rn activity in the wave-mixed region of the porous medium ($-h > z > -h - \zeta$) is equivalent to ^{222}Rn activity in the surface water ($z > -h$), wave-forced $q_{bf.w}$ will not load surface waters with ^{222}Rn, and SGD estimates based on ^{222}Rn balance techniques may not include wave-forced SGD. At these locations, SGD estimates made with ^{222}Rn balance techniques (1) may be underestimated by as much as $\bar{q}_{bd.w}$, and (2) may only reflect a subset of all processes that force SGD at the location, where the subset only contains processes that transport ^{222}Rn.

Consider an abrupt geologic transition in space from the hydrogeologic unit described in Table 4 to the 0.3–m-thick unit described in Table 5. Using the Case II model, $\lambda_r \hat{h} = 1.2$ generates $\hat{P}_{II} = 0.8$ (Equation 33), for the 1 s wave. The abrupt transition reduces $\hat{A}_I = 0.51$ for this wave to $\hat{A}_{II} = 0.43$, $\alpha_I = 36.1\ cm/d$ to $\alpha_{II} = 30.6\ cm/d$, and $\bar{q}_{bd.w.I} = 11.5\ cm/d$ to $\bar{q}_{bd.w.II} = 9.7\ cm/d$. The geologic transition reduces α and $\bar{q}$ by $\hat{P}_{II} = 0.8$.

If the hypothetical 2–dpm/l activity exists at this location, $Q_{bd.I} = 230\, dpm/m^2d$ reduces to $Q_{bd.II} = 195\, dpm/m^2d$ across the transition, for the 1 s wave. The hydrogeologic unit of finite thickness damps $q_{bf.w}$ as waves cross the abrupt geologic transition.

Consider an alternate abrupt geologic transition in space, from the hydrogeologic unit described in Table 4 to the dual-unit system described in Table 6, where the upper layer is $0.2\, m$ thick with $k_1 = 10^{-11} m^2$ and the lower layer is more permeable, with $k_2 = 10^{-10} m^2$, such that $(k_2/k_1) = 10$. This quasi-confined, Case III system ($[k_2/k_1] > 1$, Figure 3A) may exist in a region with karst geology; on a coral reef; or in clastic settings, where a veneer of finer estuarine sediment overlies coarser sediment. As the 1 s wave crosses the abrupt transition, the quasi-confined stratigraphy increases $\hat{A}_I = 0.51$ to $\hat{A}_{III} = 0.70$, $\alpha_I = 36.1\, cm/d$ to $\alpha_{III} = 49.4\, cm/d$, and $\bar{q}_{bd.w.I} = 11.5\, cm/d$ to $\bar{q}_{bd.w.III} = 15.7\, cm/d$. This transition increases α and $\bar{q}$ for this wave by $\hat{P}_{III} = 1.4$. If the hypothetical 2–dpm/l activity exists at this location, the abrupt transition increases $Q_{bd.I} = 230\, dpm/m^2d$ to $Q_{bd.III} = 315\, dpm/m^2d$, for the $1\, s$ wave. One potential consequence of the quasi-confined, Case III system is that benthic constituent fluxes driven by waves in karst, coral reef, or clastic regions may be elevated when compared to neighboring regions, with similar wave climates and bed-surface geology.

8. Wave-Forced Benthic Flux May Confound Traditional SGD Observational Techniques

Consider a transient wave climate that forces a transient $q_{bf.w}$ signal. In addition, consider an SGD estimate based on a tracer concentration χ made in a well, at a depth $z \ll -h - \zeta_{max}$, where ζ_{max} is associated with the most aggressive wave that occurs during the observation. Wave-forced $q_{bf.w}$ will not affect χ at the sampling location because the wave-forced velocity field does not penetrate deeper than $z = -h - \zeta_{max}$. The SGD estimate made with χ will not incorporate wave-forced $q_{bf.w}$ because χ is taken at $z \ll -h - \zeta_{max}$, beyond the influence of the wave. SGD estimates made with tracer concentrations taken at depths beyond the influence of waves (1) may underestimate SGD by as much as $\bar{q}_{bd.w}$, and (2) may only reflect a subset of all processes that force SGD at the location, where the subset contains processes that transport χ.

Lee [1977, Figure 3] observed a flux asymmetry in laboratory tests of the Lee-type seepage meter. *Lee* [1977] generated a series of positive and negative, steady-state hydraulic gradients i in a laboratory setting and measured seepage velocities, $q_{bd.w}$ and $q_{br.w}$, with a manual seepage meter. *Lee* [1977] observed that a plot of q versus i displayed two distinct, linear trends

$$q_{bf.w} = \begin{cases} q_{bd.w} \approx 19.1i, & i > 0 \\ q_{br.w} \approx 11.7i, & i < 0 \end{cases} \tag{58}$$

where $q_{bf.w}$, $q_{bd.w}$, and $q_{br.w}$ in Equation 58 are not forced by waves. *Lee* [1977] explained the flux asymmetry by suggesting that fine sediment is deposited on the bed when $i < 0$ and suspended when $i > 0$. The flux asymmetry ratio

$$\mathcal{C} = \frac{q_{br.w}}{q_{bd.w}} \tag{59}$$

can be used to estimate a seepage-meter, flux-asymmetry error

$$\begin{aligned} \epsilon &= \bar{q}_{bd.w} + \mathcal{C}\bar{q}_{br.w} \\ &= \bar{q}_{bd.w}(1 - \mathcal{C}) \end{aligned} \tag{60}$$

Where a seepage meter is flux symmetric, $\mathcal{C} = 1$ and $\epsilon = 0$.

Consider the small-amplitude wave climate described in Table 4 and assume $\mathcal{C} \approx 11.7/19.1 = 0.6$ from *Lee*'s [1977] observation (Equation 58). The assumed asymmetry error $\epsilon = 4.5\, cm/d$ will fill a one-liter measurement bag attached to a traditional, Lee-type, manual seepage meter in $2.1\, hr$.

Lee [1977] investigated steady-state i; he did not consider wave-forced oscillatory loading. Wave-forced flux asymmetries may differ from the $\mathcal{C} = 0.6$ estimated with Equation 58. For example, the oscillatory q_{bf} may suspend the fine sediments that caused *Lee*'s (1977) asymmetry under the steady-state i. The interior of the seepage meter is not exposed to the bed-parallel currents, which exist outside the meter. These currents may play an important role in suspending fine sediments outside the meter. The absence of these currents inside the meter may enable the asymmetry. This simplistic analysis should not be interpreted as conclusive evidence that small-amplitude waves undermine the utility of the seepage meter, at all locations. *Lee*'s (1977) asymmetry and this simplistic analysis suggest that the seepage meter should be subjected to detailed, controlled, documented, repeatable laboratory experiments, in which this asymmetry and the performance of the seepage meter are fully investigated under an array of wave forcings and sediment distributions.

Consider a Lee-type, manual seepage meter deployed at a location where the sediment distribution causes the meter to operate in a flux-symmetric manner ($\mathcal{C} = 1$ and $\epsilon = 0$). This flux-symmetric deployment will not measure waved-forced $q_{bf.w}$ because the $q_{bf.w}$ signal integrates to zero over integer multiples of one wave period (Equation 54). SGD estimates made with a flux-symmetric seepage meter may underestimate SGD by as much as $\bar{q}_{bd.w}$.

If the valve that connects the measurement bag to the seepage chamber is one-way, such that flow from the bag to the chamber is prohibited (a discharge-only orientation), then

$\mathcal{C} = 0$ and $\epsilon = \bar{q}_{bd.w}$. If forcing is limited to waves, then the seepage meter may measure wave-forced $\bar{q}_{bd.w}$ with the discharge-only orientation. It may be possible to deduce wave-forced SGD with a trio of deployed seepage meters: one discharge-only orientation, one-recharge only orientation, and one traditional discharge-recharge orientation. These observational strategies require laboratory validation.

9. Conclusions

A generalized analytical model for wave-forced $q_{bf.w}$ over a series of rigid hydrogeologic units is developed by modifying a boundary value problem by *Reid and Kajiura* [1957]. Solutions for hydrogeologic units of infinite and finite thickness, and for a dual-unit system are shown to be congruent, with convergent values of $\hat{h}$ and k. *Yamamoto et al.*'s [1978] observations of $|p(z < -h)|/p(z = -h)$ in a laboratory flume match the Case II solution (Figure 4).

A dimensionless amplitude parameter $\hat{A}$ is introduced for wave-forced $q_{bf.w}$. It is shown that $\hat{A}$ is maximized for an intermediate-depth wave, with $\lambda_r h = 1.2$; and that $\hat{A}$ decreases from this maximum (1) on $\lambda_r h > 1.2$ because wave orbitals lose contact with the bed, and (2) on $\lambda_r h < 1.2$ because the pressure distribution becomes hydrostatic. For the same wave climate ($\lambda_r h$), both $q_{bf.w}$ for the hydrogeologic unit of finite thickness and $q_{bf.w}$ for the quasi-finite, dual-unit system are less than $q_{bf.w}$ for the hydrogeologic unit of infinite thickness ($q_{bf.w.II} < q_{bf.w.I}$ and quasi-finite $q_{bf.w.III} < q_{bf.w.I}$). For the same wave climate ($\lambda_r h$), $q_{bf.w}$ for the quasi-confined, dual-unit system is greater than $q_{bf.w}$ for the hydrogeologic unit of infinite thickness (quasi-confined $q_{bf.w.III} > q_{bf.w.I}$). Case II damps $q_{bf.w.I}$; the quasi-finite, Case III system damps $q_{bf.w.I}$; the quasi-confined, Case III system amplifies $q_{bf.w.I}$. The potential for wave-driven $q_{bf.w}$ amplification by quasi-confined systems suggests that benthic constituent fluxes may be greater in quasi-confined systems than in neighboring regions without quasi-confinement. The quasi-confined system may exist in regions with karst geology, on coral reefs, or in clastic settings.

Seepage meters and tracers may not accurately measure wave-forced $q_{bf.w}$ at all locations. SGD estimates based on tracer concentrations that are collected at depths below the wave-forced velocity field may not register the influence of wave-forced $q_{bf.w}$. Where a tracer exhibits equivalent, representative concentrations in both the surface water near the bed and in the wave-mixed region of the porous medium, wave-forced $q_{bf.w}$ may not transport a net load from the porous medium into the surface water. SGD estimates based on tracer conservation statements at these locations may underestimate SGD by as much as $\bar{q}_{bd.w}$. *Lee* [1977] showed that the flux response of the Lee-type, manual seepage meter is asymmetrical, under certain conditions. At some locations, a sediment distribution may exist that enables *Lee*'s (1977) asymmetry, such that wave-forced $q_{bf.w}$ pumps water into the seepage meter. It was shown that a $T = 1\ s$, $a = 5\ cm$ wave forces an $11.5\ cm/d$ SGD in $0.5\ m$ of water; and that if a $\mathcal{C} = 0.6$ flux asymmetry exists at this location, wave-forced $q_{bf.w}$ will fill a one liter measurement bag attached to a standard, Lee-type seepage meter, in $2.1 hr$. Where the seepage meter is flux-symmetric, the seepage meter may not be capable of measuring wave-forced $q_{bd.w}$ due the symmetrical $q_{bf.w}$ signal (Equation 54). Laboratory experiments should be performed to investigate *Lee*'s (1977) asymmetry under an array of wave forcings and sediment distributions.

Appendix

Case I:

$$A = \frac{\imath C}{\sigma\rho} \tag{A1}$$

$$B = \frac{Ck}{\mu} \tag{A2}$$

$$C = \frac{\rho g a}{\cosh(\lambda h)\left[1 - \imath R \tanh(\lambda h)\right]} \tag{A3}$$

Case II:

$$A = \frac{\imath C}{\sigma\rho}\cosh(\lambda\hat{h}) \tag{A4}$$

$$B = \frac{Ck}{\mu}\sinh(\lambda\hat{h}) \tag{A5}$$

$$C = \frac{\rho g a}{\cosh(\lambda h)\cosh(\lambda\hat{h})\left[1 - \imath R \tanh(\lambda h)\tanh(\lambda\hat{h})\right]} \tag{A6}$$

$$D = 0 \tag{A7}$$

Case III:

$$A = \frac{\imath\left[C\cosh(\lambda\hat{h}) + D\sinh(\lambda\hat{h})\right]}{\sigma\rho} \tag{A8}$$

$$B = \frac{k_1}{\mu}\left[C\sinh(\lambda\hat{h}) + D\cosh(\lambda\hat{h})\right] \tag{A9}$$

$$C = E \tag{A10}$$

$$D = \frac{k_2}{k_1}E \tag{A11}$$

$$E = \frac{\rho g a}{\cosh(\lambda h)\cosh(\lambda\hat{h})} \times \frac{1}{\left[1 + \frac{k_2}{k_1}\tanh(\lambda\hat{h}) - \imath R_1 \tanh(\lambda h)\left[\tanh(\lambda\hat{h}) + \frac{k_2}{k_1}\right]\right]} \tag{A12}$$

Notation

^{222}Rn Radon-222.

A unknown in boundary value problem, $[L^2T^{-1}]$.

$\hat{A}$ dimensionless amplitude parameter for $q_{bf.w}$.

A_s surface area of spherical sediment particle, $[L^2]$.

B unknown in boundary value problem, $[L^2T^{-1}]$.

C unknown in boundary value problem, $[ML^{-1}T^{-2}]$.

$\mathcal{C}$ seepage meter asymmetry ratio.

C_χ concentration of constituent χ, $[ML^{-3}]$.

$C_{bd.\chi}$ concentration of constituent χ in $q_{bd.w}$, $[ML^{-3}]$.

$C_{br.\chi}$ concentration of constituent χ in $q_{br.w}$, $[ML^{-3}]$.

D unknown in boundary value problem, $[ML^{-1}T^{-2}]$.

E unknown in boundary value problem, $[ML^{-1}T^{-2}]$.

$[F]$ force dimension.

L wave length, $[L]$.

$[L]$ linear dimension.

M_s specific surface of spherical sediment particle, $[L^{-1}]$.

$[M]$ mass dimension.

$O(\diamond)$	order of magnitude of some parameter $\diamond$.
$\hat{P}$	dimensionless, generalized $q_{bf.w}$ model parameter.
$\hat{Q}$	dimensionless, generalized $q_{bf.w}$ model parameter.
Q_χ	rate at which a surface-water body is loaded with a constituent χ, $[ML^{-2}T^{-1}]$.
R	*Reid and Kajiura*'s [1957] fundamental dimensionless permeability modulus.
$\Re$	real part of a complex number.
T	wave period, $[T]$.
$[T]$	time dimension.
V_s	volume of spherical sediment particle, $[L^3]$.
a	amplitude of linear water wave, $[L]$.
$\bar{d}$	mean diameter of sediment particle, $[L]$.
e	$= 2.71828183\ldots$.
f	a dimensionless function.
g	gravitational acceleration, $[LT^{-2}]$.
h	mean surface-water depth, $[L]$.
$\hat{h}$	hydrogeologic-unit thickness, $[L]$.

i hydraulic gradient, $[LL^{-1}]$.

$\imath$ imaginary number, $\imath = \sqrt{-1}$.

k permeability, $[L^2]$.

k_2/k_1 dimensionless permeability ratio.

n porosity, $[L^3L^{-3}]$.

p dynamic pressure, $[FL^{-2} = ML^{-1}T^{-2}]$.

p_{static} static pressure, $[FL^{-2} = ML^{-1}T^{-2}]$.

p_{total} total pressure, $[FL^{-2} = ML^{-1}T^{-2}]$.

p_{pm} dynamic pore pressure, $[FL^{-2} = ML^{-1}T^{-2}]$.

q_{bd} benthic discharge flux, property specific units: for example, $[L^3T^{-1}L^{-2} = LT^{-1}]$ for a benthic volume discharge flux, $[MT^{-1}L^{-2}]$ for a benthic mass discharge flux.

q_{bf} benthic flux, property specific units.

q_{br} benthic recharge flux, property specific units,

$q_{bd.w}$ benthic water discharge flux, $[LT^{-1}]$.

$\bar{q}_{bd.w}$ average benthic water discharge flux over one wave period, $[LT^{-1}]$.

$q_{bf.w}$ benthic water flux, $[LT^{-1}]$.

$\bar{q}_{bf.w}$ average benthic water flux over one wave period, $[LT^{-1}]$.

$q_{bf.w.nd}$ dimensionless $q_{bd.w}$.

$q_{br.w}$ benthic water recharge flux, $[LT^{-1}]$.

$\bar{q}_{br.w}$ average benthic water recharge flux over one wave period, $[LT^{-1}]$.

t time, $[T]$.

w vertical velocity, $[LT^{-1}]$.

w_{pm} vertical velocity in the porous medium, $[LT^{-1}]$.

x Cartesian horizontal dimension, $[L]$.

z Cartesian vertical dimension, $[L]$.

α amplitude of $q_{bf.w}$, $[L]$.

β dimensionless amplification parameter for $q_{bf.w}$.

ϵ seepage meter flux asymmetry error, $[LT^{-1}]$.

ζ thickness of the region of porous medium over which a wave-forced velocity field transports constituents, $[L]$.

η water surface displacement about $z = 0$, $[L]$.

λ wave number, $[L^{-1}]$.

$\lambda_\imath$ wave number, imaginary component, $[L^{-1}]$.

λ_r wave number, real component, $[L^{-1}]$.

$\lambda_r h$ dimensionless depth.

$\lambda_r \hat{h}$ dimensionless hydrogeologic-unit thickness.

μ dynamic viscosity of water, $[FTL^{-2} = ML^{-1}T^{-1}]$.

ν kinematic viscosity of water, $[L^2T^{-1}]$.

π $= \arccos(-1)$.

ρ density of water, $[ML^{-3}]$.

σ wave radial frequency, $\sigma = (2\pi)/(T)$, $[L^{-1}]$.

ϕ velocity potential, $[L^2T^{-1}]$.

$\nabla^2(\diamond)$ two-dimensional Laplacian operator on some parameter $\diamond$, where $\nabla^2(\diamond) = (\partial^2\diamond)/(\partial x^2) + (\partial^2\diamond)/(\partial z^2)$.

∞ infinity.

Subscripts:

0 parameter at the bed.

1 hydrogeologic unit bounded by $z = -h$.

2 hydrogeologic unit with top interface bounded by Unit 1.

I Case I.

II Case II.

III Case III.

bd benthic discharge.

bf benthic flux.

br benthic recharge.

$\imath$ imaginary component of imaginary number.

j hydrogeologic unit counter.

nd dimensionless.

pm porous medium variable.

r real component of imaginary number.

w water.

χ hypothetical constituent.

Acknowledgments. We are grateful to JF Bratton, SC Cooper, KJ Cunningham, MG Deacon, NR deSieyes, AS Harrison, LG Larsen, HA Michael, CD Reich, RA Renken, WE Sanford, and PW Swarzenski for insight and expertise. We also appreciate the efforts of JT Kirby and three anonymous reviewers in vetting this manuscript. This work was partially funded by the U.S. Geological Survey, Water Resources Discipline.

References

Bear, J. (1988), *Dynamics of fluids in porous media*, 764 pp., Dover Publications, New York, New York, USA.

King, J. N. (2007), *Selective mechanisms for benthic water flux generation in coastal waters*, PhD Dissertation, University of Florida, Gainesville, Florida, USA.

Lee, D. R. (1977), Device for measuring seepage flux in lakes and estuaries, *Limnology and Oceanography*, *22*(1), 140–147.

Martin, J. B., J. E. Cable, J. Jaeger, K. Hartl, and C. G. Smith (2006), Thermal and chemical evidence for rapid water exchange across the sediment-water interface by bioirrigation in the Indian River Lagoon, Florida, *Limnology and Oceanography*, *51*(3), 1332–1341.

Pilditch, C. A., and D. C. Miller (2006), Phytoplankton deposition to permeable sediments under oscillatory flow: Effects of ripple geometry and resuspension, *Continental Shelf Research*, *26*(15), 1806–1825.

Precht, E., and M. Huettel (2003), Advective pore-water exchange driven by surface gravity waves and its ecological implications, *Limnology and Oceanography*, *48*(4), 1674–1684.

Precht, E., and M. Huettel (2004), Rapid wave-driven advective pore water exchange in a permeable coastal sediment, *Journal of Sea Research*, *51*(2), 93–107.

Precht, E., U. Franke, L. Polerecky, and M. Huettel (2004), Oxygen dynamics in permeable sediments with wave-driven pore water exchange, *Limnology and Oceanography*, *49*(3), 693–705.

Reid, R. O., and K. Kajiura (1957), On the damping of gravity waves over a permeable sea bed, *Transactions, American Geophysical Union*, *38*(5), 662–666.

Riedl, R. J., N. Huang, and R. Machan (1972), The subtidal pump: a mechanism of interstitial water exchange by wave action, *Marine Biology*, *13*, 210–221.

Shum, K. T. (1992), Wave-induced advective transport below a rippled water-sediment interface, *Journal of Geophysical Research-Oceans*, *97*(C1), 789–808.

Sleath, J. F. A. (1970), Wave-induced pressures in beds of sand, *Proceedings of the American Society of Civil Engineers—Journal of the Hydraulics Division*, *96*(2), 367–378.

Taniguchi, M., W. C. Burnett, J. E. Cable, and J. T. Turner (2002), Investigation of submarine groundwater discharge, *Hydrological Processes*, *16*, 2115–2129.

Yamamoto, T., H. L. Koning, H. Sellmeijer, and E. P. Van Hijum (1978), Response of a poro-elastic bed to water-waves, *Journal of Fluid Mechanics*, *87*, 193–206.

Table 1. Dimensionless model coefficients.

	hydrogeologic unit thickness			
case	surficial	underlying	$\hat{P}$	$\hat{Q}$
I	∞	-	1	0
II	$\hat{h}$	-	$\tanh(\lambda_r \hat{h})$	$\frac{2\lambda_i \hat{h}}{\sinh(2\lambda_r \hat{h})}$
III	$\hat{h}$	∞	$\frac{\tanh(\lambda_r \hat{h})+\frac{k_2}{k_1}}{\frac{k_2}{k_1}\tanh(\lambda_r \hat{h})+1}$	$\frac{\lambda_i \hat{h}(1-\frac{k_2}{k_1})\left[1-\tanh^2(\lambda_r \hat{h})\right]}{\left[\frac{k_2}{k_1}\tanh(\lambda_r \hat{h})+1\right]\left[\tanh(\lambda_r \hat{h})+\frac{k_2}{k_1}\right]}$

Table 2. Model input and derived sediment parameters for the application of Case II to *Yamamoto et al.*'s [1978] laboratory observations, where $\bar{d}$ is mean sediment diameter, A_s surface area of sediment sphere, V_s volume of sediment sphere, and M_s is specific surface of the sediment sphere.

parameter	value	unit	note
n	0.4		canonical value
ρ	1000	kg/m^3	canonical value
ν	1.12×10^{-6}	m^2/s	canonical value
h	0.90	m	given by *Yamamoto et al.* [1978]
$\hat{h}$	0.50	m	given by *Yamamoto et al.* [1978]
$\bar{d}$	1.2	mm	given by *Yamamoto et al.* [1978]
A_s	4.52×10^{-6}	m^2	$= \pi \bar{d}^2$
V_s	9.05×10^{-10}	m^3	$= \pi \bar{d}^3/6$
M_s	5000	m^{-1}	$= A_s/V_s$
			Bear [1988, Equation 2.6.4]
k	1.42×10^{-9}	m^2	$= n^3/\left[5M_s^2(1-n)^2\right]$
			Kozeny-Carman Equation
			Bear [1988, Equation 5.10.18]

Table 3. Model output parameters for the application of Case II to *Yamamoto et al.*'s [1978] laboratory observations.

	$T[s]$					
parameter	2.6	2.0	1.5	1.0	unit	note
σ	2.42	3.14	4.19	6.28	s^{-1}	$= 2\pi/T$
R	3.1×10^{-3}	4.0×10^{-3}	5.3×10^{-3}	8.0×10^{-3}		Equation 16
λ_r	0.89	1.25	1.91	4.03	m^{-1}	Equation 18
L	7.03	5.04	3.29	1.56	m	$= 2\pi/\lambda_r$
$\lambda_r h$	0.80	1.12	1.72	3.63		
$\lambda_r \hat{h}$	0.45	0.62	0.95	2.02		
$\hat{P}$	0.42	0.55	0.74	0.97		Equation 33
$\lambda_\imath$	5.7×10^{-4}	8.0×10^{-4}	7.9×10^{-4}	8.6×10^{-5}	m^{-1}	Equation 34
$\hat{Q}$	5.6×10^{-4}	5.0×10^{-4}	2.4×10^{-4}	3.1×10^{-6}		Equation 38

Table 4. Hypothetical application of Case I.

parameter	value			unit	note
general inputs					
T	1	5	10	s	
a	0.050	0.233	0.611	m	
g	9.8	9.8	9.8	m/s^2	
k	1×10^{-11}	1×10^{-11}	1×10^{-11}	m^2	
ρ	1030	1030	1030	kg/m^3	
ν	1.2×10^{-6}	1.2×10^{-6}	1.2×10^{-6}	m^2/s	
h	0.5	2.5	5.0	m	
$C_{bd.^{222}Rn}$	2	2	2	dpm/l	
$C_{br.^{222}Rn}$	0	0	0	dpm/l	
general outputs					
σ	6.3	1.3	0.6	$1/s$	$= 2\pi/T$
λ_r	4.2	0.27	0.093	$1/m$	Equation 18
L	1.51	23.1	67.6	m	$= 2\pi/\lambda_r$
$\lambda_r h$	2.1	0.68	0.46		
R	5×10^{-5}	1×10^{-5}	5×10^{-6}		Equation 16
Case I outputs					
$\hat{P}_I$	1.0	1.0	1.0		Table 1
$\lambda_{\imath.I}$	1×10^{-5}	2×10^{-6}	5×10^{-7}	$1/m$	Equation 19
$\hat{Q}_I$	0.0	0.0	0.0		Table 1
β_I	5×10^{-5}	1×10^{-5}	6×10^{-6}		Equation 15
$\hat{A}$	0.51	0.55	0.42		Equation 52
α_I	4.2×10^{-6}	4.2×10^{-6}	4.2×10^{-6}	m/s	Equation 14
	36.1	36.1	36.1	cm/d	
$\bar{q}_{bd.w.I}$	1.3×10^{-6}	1.3×10^{-6}	1.3×10^{-6}	m/s	Equation 55
	11.5	11.5	11.5	cm/d	
$Q_{bd.I}$ for ^{222}Rn	2.7×10^{-3}	2.7×10^{-3}	2.7×10^{-3}	dpm/m^2s	Equation 57
	230	230	230	dpm/m^2d	

Table 5. Hypothetical application of Case II, where additional inputs and case-independent outputs are detailed in Table 4.

parameter	value	unit	note
additional Case II inputs			
$\hat{h}$	0.3	m	
Case II outputs			
$\lambda_r \hat{h}$	1.2		
$\hat{P}_{II}$	0.8		Table 1
$\lambda_{\imath.II}$	1×10^{-5}	$1/m$	Equation 19
$\hat{Q}_{II}$	1×10^{-6}		Table 1
β_{II}	4×10^{-5}		Equation 15
$\hat{A}_{II}$	0.43		Equation 52, Figure 5
α_{II}	3.5×10^{-6}	m/s	Equations 14 and 52
	30.6	cm/d	
$\bar{q}_{bd.w.II}$	1.1×10^{-6}	m/s	Equation 55
	9.7	cm/d	
$Q_{bd.II}$ for ^{222}Rn	2.3×10^{-3}	$dpm/(m^2 s)$	Equation 57
	195	$dpm/(m^2 d)$	

Table 6. Hypothetical application of Case III, where additional inputs and case-independent outputs are detailed in Table 4.

parameter	value	unit	note
additional Case III inputs			
$\hat{h}$	0.2	m	
k_1	1×10^{-11}	m^2	
k_2	1×10^{-10}	m^2	
Case III outputs			
$\lambda_r \hat{h}$	0.8		
k_2/k_1	10		
$\hat{P}_{III}$	1.4		Table 1
$\lambda_{\imath.III}$	1×10^{-5}	$1/m$	Equation 19
$\hat{Q}_{III}$	-1×10^{-7}		Table 1
β_{III}	7×10^{-5}		Equation 15
$\hat{A}_{III}$	0.70		Equation 52, Figure 6C
α_{III}	5.7×10^{-6}	m/s	Equations 14 and 52
	49.4	cm/d	
$\bar{q}_{bd.w.III}$	1.8×10^{-6}	m/s	Equation 55
	15.7	cm/d	
$Q_{bd.III}$ for ^{222}Rn	3.6×10^{-3}	$dpm/(m^2 s)$	Equation 57
	315	$dpm/(m^2 d)$	

Figure 1. A two-dimensional, vertically-oriented cross section—in x and z dimensions—of wave-forced $q_{br.w}$ and $q_{bd.w}$, with a water surface at $z = \eta$ oscillating about a still-water surface at $z = 0$. The bed of the water-body is located at $z = -h$. The following domain geometry is used to solve two-dimensional boundary value problems in the current work: (A) Case I: hydrogeologic unit of infinite thickness; (B) Case II: hydrogeologic unit of finite thickness; (C) Case III: dual-unit system, which consists of a unit of finite thickness over a unit of infinite thickness. The wave-forced velocity field transports constituents within the porous domain, over $-h > z > -h - \zeta$.

Figure 2. Dimensionless benthic flux and dimensionless surface-water displacement versus dimensionless phase position, for benthic flux amplification parameter between 0 and 1.

Figure 3. Stratigraphy that represents (A) quasi-confined system: a low permeability hydrogeologic unit over a high permeability hydrogeologic unit (permeability ratio greater than unity), and (B) quasi-finite system: a high permeability hydrogeologic unit over a low permeability hydrogeologic unit (permeability ratio less than unity).

Figure 4. Depth versus ratio of the amplitude of the pressure signal at depth to the amplitude of the pressure signal at the bed $|p|/p_0$ for 1.0 (diamonds), 1.5 (squares), 2.0 (triangles), and 2.6s (circles) wave periods, where symbols are from *Yamamoto et al.*'s [1978] laboratory observations of a coarse-grained medium and lines are generated with Equation 51.

Figure 5. Dimensionless benthic flux amplitude parameter versus dimensionless depth for dimensionless hydrogeologic unit depths from 0.01 to ∞, where dimensionless hydrogeologic unit depth approaching ∞ represents Case I and dimensionless hydrogeologic unit depth less than ∞ represents Case II.

Figure 6. Dimensionless benthic flux amplitude parameter versus dimensionless depth for dimensionless hydrogeologic unit depths from 0.01 to ∞, for four permeability ratios (A) 0.01, (B) 0.1, (C) 10, (D) 100, where dimensionless hydrogeologic unit depth approaching ∞ represents Case I and dimensionless hydrogeologic unit depth less than ∞ represents Case III.

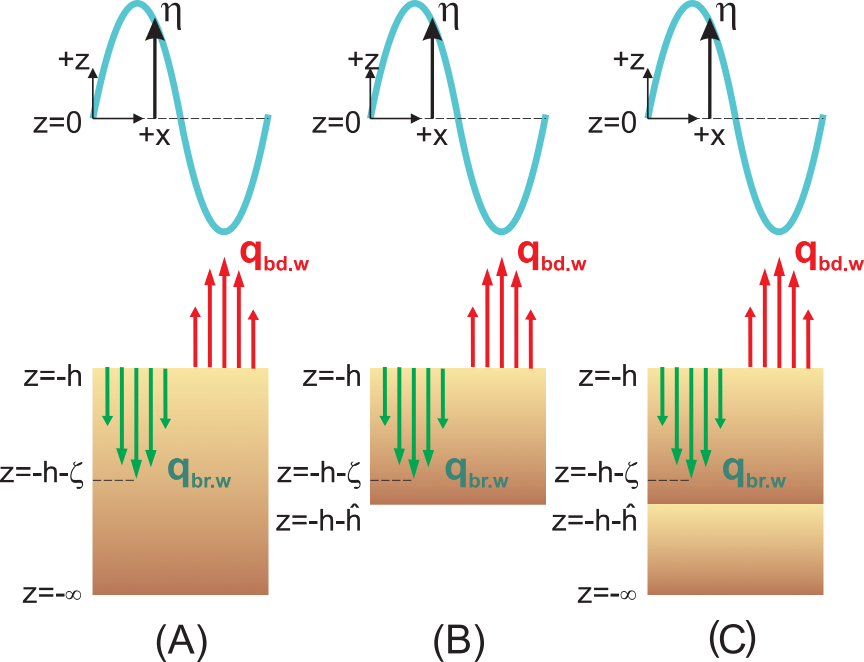

η
+z
z=0
+x
q_bd.w
z=-h
z=-h-ζ
q_br.w
z=-h-ĥ
z=-∞
(A)
(B)
(C)

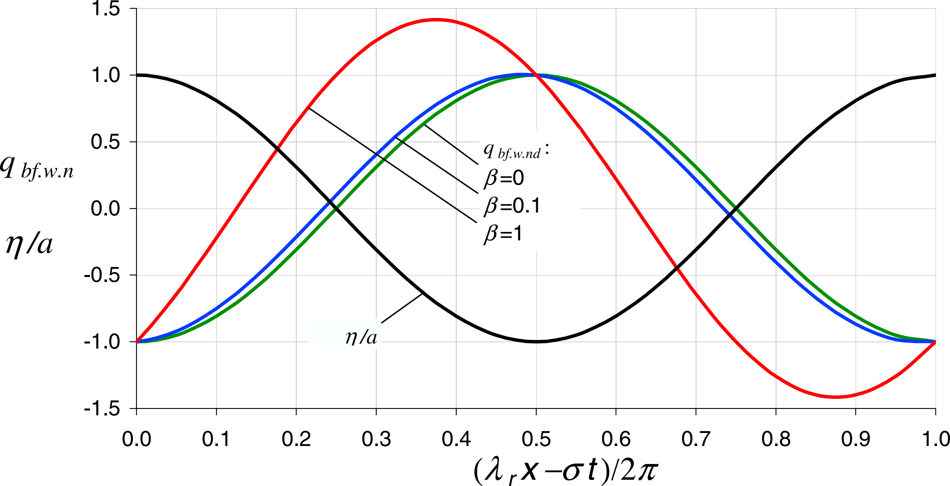

1.5
1.0
0.5
0.0
-0.5
-1.0
-1.5
q bf.w.n
η /a
q bf.w.nd :
β=0
β=0.1
β=1
η /a
0.0
0.1
0.2
0.3
0.4
0.5
0.6
0.7
0.8
0.9
1.0
(λ r x −σ t)/2π

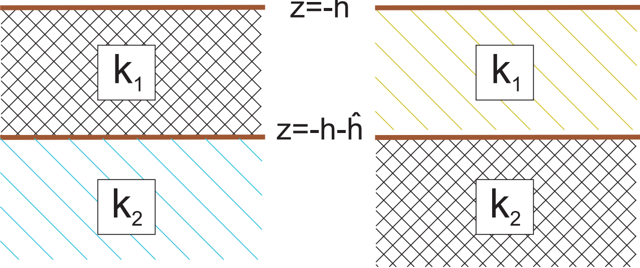

(A) quasi-confined
$k_2/k_1>1$

(B) quasi-finite
$k_2/k_1<1$

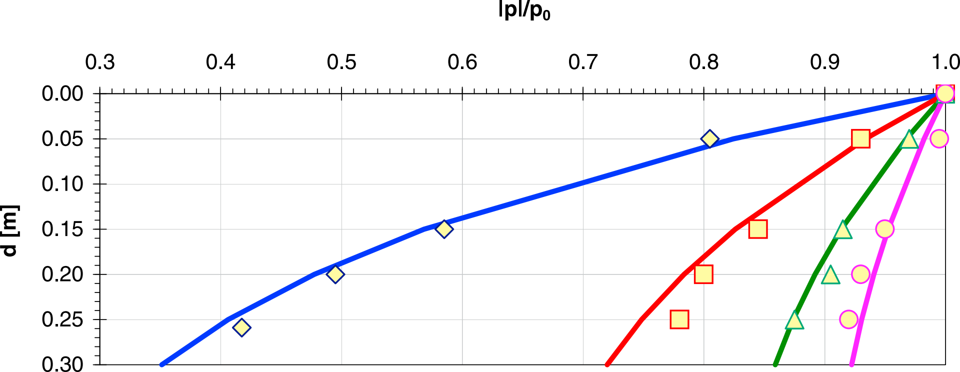

|p|/p0
0.3
0.4
0.5
0.6
0.7
0.8
0.9
1.0
0.00
0.05
0.10
0.15
0.20
0.25
0.30
d [m]

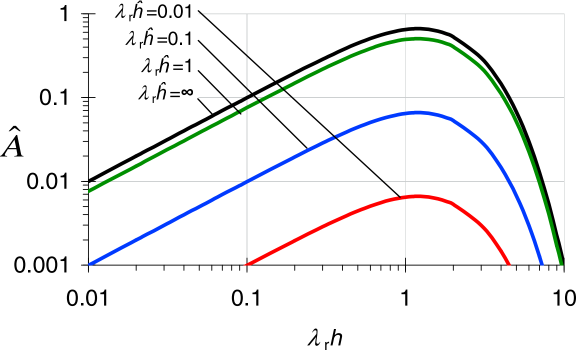

$\lambda_r\hat{h}=0.01$
$\lambda_r\hat{h}=0.1$
$\lambda_r\hat{h}=1$
$\lambda_r\hat{h}=\infty$
1
0.1
0.01
0.001
$\hat{A}$
0.01
0.1
1
10
$\lambda_r h$

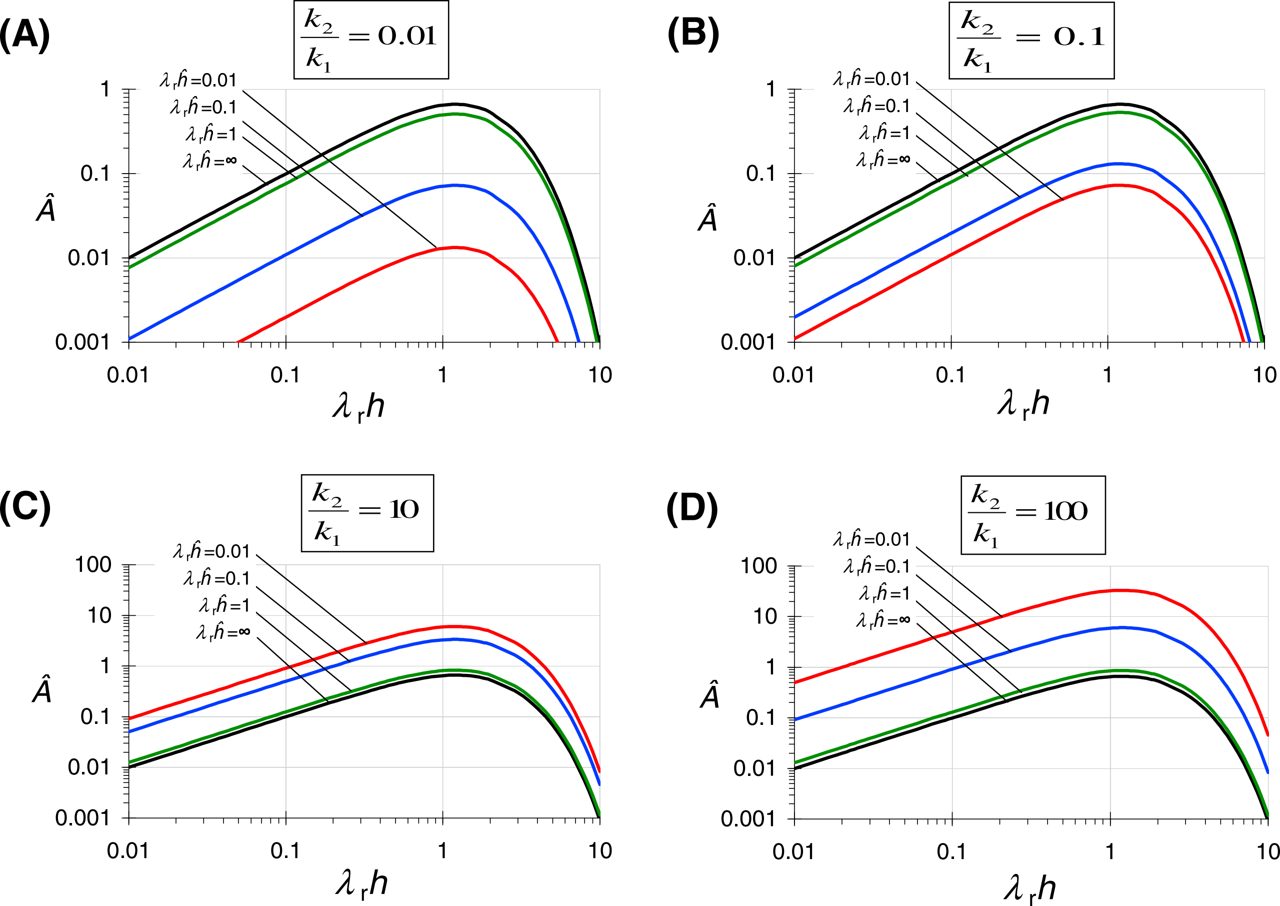

(A)
$\frac{k_2}{k_1} = 0.01$
(B)
$\frac{k_2}{k_1} = 0.1$
(C)
$\frac{k_2}{k_1} = 10$
(D)
$\frac{k_2}{k_1} = 100$
$\lambda_r \hat{h} = 0.01$
$\lambda_r \hat{h} = 0.1$
$\lambda_r \hat{h} = 1$
$\lambda_r \hat{h} = \infty$
$\hat{A}$
$\lambda_r h$
0.001
0.01
0.1
1
10
100